JOURNAL OF THE MECHANICAL BEHAVIOR OF BIOMEDICAL MATERIALS 62 (2016) 169–181

Available online at www.sciencedirect.com

ScienceDirect

www.elsevier.com/locate/jmbbm

Research Paper

Influence of structural load-bearing scaffolds on mechanical load- and BMP-2-mediated bone regeneration

Anna M. McDermott[a], *Devon E. Mason*[a], *Angela S.P. Lin*[b], *Robert E. Guldberg*[b], *Joel D. Boerckel*[a,*]

[a]*Department of Aerospace and Mechanical Engineering, Bioengineering Graduate Program, University of Notre Dame, Notre Dame, IN 46556, USA*

[b]*Woodruff School of Mechanical Engineering, Georgia Institute of Technology, Atlanta, GA 30332, USA*

ARTICLE INFO

Article history:
Received 1 March 2016
Received in revised form
4 May 2016
Accepted 5 May 2016
Available online 12 May 2016

Keywords:
Bone defect
Mechanical loading
Scaffold
Tissue engineering

ABSTRACT

A common design constraint in functional tissue engineering is that scaffolds intended for use in load-bearing sites possess similar mechanical properties to the replaced tissue. Here, we tested the hypothesis that *in vivo* loading would enhance bone morphogenetic protein-2 (BMP-2)-mediated bone regeneration in the presence of a load-bearing PLDL scaffold, whose pores and central core were filled with BMP-2-releasing alginate hydrogel. First, we evaluated the effects of *in vivo* mechanical loading on bone regeneration in the structural scaffolds. Second, we compared scaffold-mediated bone regeneration, independent of mechanical loading, with alginate hydrogel constructs, without the structural scaffold, that have been shown previously to facilitate *in vivo* mechanical stimulation of bone formation.

Contrary to our hypothesis, mechanical loading had no effect on bone formation, distribution, or biomechanical properties in structural scaffolds. Independent of loading, the structural scaffolds reduced bone formation compared to non-structural alginate, particularly in regions in which the scaffold was concentrated, resulting in impaired functional regeneration.

This is attributable to a combination of stress shielding by the scaffold and inhibition of cellular infiltration and tissue ingrowth. Collectively, these data question the necessity of scaffold similarity to mature tissue at the time of implantation and emphasize development of an environment conducive to cellular activation of matrix production and ultimate functional regeneration.

Abbreviations: PLDL, co-polymer of poly(L-lactide) and poly(DL-lactide); ALG, alginate; RGD, arginine, glycine, aspartic acid-containing peptide; PCL, poly(ε-caprolactone); BMP-2, Bone morphogenetic protein-2; microCT, microcomputed tomography

*Correspondence to: University of Notre Dame, Multidisciplinary Research Building, Rm 142, Notre Dame, IN 46556, USA. Tel.: +1 574 631 1866.

E-mail address: jboercke@nd.edu (J.D. Boerckel).

http://dx.doi.org/10.1016/j.jmbbm.2016.05.010
1751-6161/

1. Introduction

Mechanical stimuli have long been implicated as critical regulators of bone structure and behavior (Wolff, 1892). Mechanical loads control nearly all aspects of bone development, homeostasis, and disease, including load-induced bone modeling and remodeling (Robling and Turner, 2009), disuse-associated osteopenia (Turner et al., 2009), and peri-implant resorption caused by stress shielding (Duyck and Vandamme, 2014). The process of fracture healing is also acutely sensitive to mechanical stimuli, with both the magnitude and mode of interfragmentary motion influencing tissue differentiation, speed of recovery, and ultimate clinical outcome (Kenwright et al., 1986; Röntgen et al., 2010; Wolf et al., 1998).

The consensus of many experimental (Claes et al., 1998; Goodship and Kenwright, 1985; Roux, 1895) and theoretical (Carter et al., 1996; Claes and Heigele, 1999; Lacroix and Prendergast, 2002; Pauwels, 1960; Perren and Cordey, 1980) studies on bone fracture healing demonstrates that cellular lineage specification and tissue differentiation in the fracture callus is controlled by local mechanical conditions, with thresholds and modes of interfragmentary stress and strain regulating callus formation and remodeling. However, the conditions necessary for functional regeneration of critical sized bone defects, which cannot heal without intervention, remain poorly understood and cannot be predicted by the classical theory alone (Claes et al., 1997, 1994; Gómez-Benito et al., 2005).

In recent years, attempts to re-engineer diseased and damaged tissues have demonstrated the importance of both intrinsic and extrinsic mechanical cues for functional regeneration. Intrinsic mechanical cues include inherent properties of the extracellular matrix such as elastic rigidity and viscoelasticity (Chaudhuri et al., 2015; Engler et al., 2006; Huebsch et al., 2015), while extrinsic cues include both static and dynamic forces applied via boundary conditions (Boerckel et al., 2011b; Guldberg et al., 1997). Each of these is of particular importance in bone tissue engineering, where tissue function is fundamentally mechanical. For example, intrinsic matrix mechanical properties are sufficient *per se* to control lineage specification of stem and progenitor cells (Engler et al., 2006), an observation that has inspired many to pursue controllable, defined matrices for use in tissue engineering, frequently through hydrogels (Huebsch et al., 2015; Kreger et al., 2010; Mason et al., 2013). Similarly, the importance of extrinsic mechanical conditions in tissue formation and adaptation is apparent in the prevalence of dynamic bioreactors for *in vitro* tissue conditioning and culture (Matziolis et al., 2006; Mauney et al., 2004; Porter et al., 2007). Efforts to control the biomechanical environment *in vivo* have also revealed profound effects of both intrinsic (Bailey et al., 2011; Huebsch et al., 2015; Jeon et al., 2009) and extrinsic (Boerckel et al., 2011b; Glatt et al., 2012; Roshan-Ghias et al., 2011, 2010) mechanical stimuli on tissue regeneration.

It has long been posited that the ideal biomaterial for tissue engineering would have identical properties to the tissue being replaced (Butler et al., 2009, 2000), balanced by other factors including microstructure, degradation, cell adhesion, and inflammation (Keane and Badylak, 2014). This principle, termed "mechanical similarity," has been particularly influential in bone tissue engineering, where a common design criterion is to match the properties of native bone, or at least enable physiologic loading without additional stabilization (Butler et al., 2009; Tang et al., 2016).

Recently, we developed a model system to evaluate the role of *in vivo* mechanical loading on large bone defect regeneration (Boerckel et al., 2009). In this model, a critically sized (8 mm) bone defect is created in the rat femur, requiring treatment to induce healing. To stimulate bone formation, we evaluated delivery of rhBMP-2 using a non-structural alginate hydrogel which released the protein over a time-course of 21 days *in vivo* (Boerckel et al., 2011a; Kolambkar et al., 2011b). We then tested the effects of *in vivo* loading and load timing on bone formation, tissue differentiation, and neovascularization by modifying the fixation plates to allow elective actuation of ambulatory load transfer through compliant fixation plates designed to constrain loading to axial compression (Boerckel et al., 2012, 2011b, 2009). These studies found that limb fixation with the compliant plates implanted in the unlocked configuration at day 0 (*i.e.* early loading) prevented vascular ingrowth and inhibited bone formation while increasing cartilage formation; however, delaying load initiation to week 4, after onset of bone formation and initiation of defect bridging, significantly enhanced bone formation, biomechanical properties, and local tissue adaptation and remodeling (Boerckel et al., 2012, 2011b, 2009).

The purpose of the present study was two-fold: first, to evaluate the influence of *in vivo* mechanical loading on large bone defect regeneration in the presence of a structural load-bearing scaffold capable of supporting and transmitting ambulatory loads to the defect, and second, to compare bone regeneration in the structural and non-structural constructs independent of mechanical stimulation. In Part 1, we tested the hypothesis that mechanical loading would enhance large bone defect regeneration in the presence of a tissue engineering scaffold featuring structural properties and microarchitectural features (*i.e.* porosity and anisotropy) similar to those of trabecular bone. In Part 2, we compared bone regeneration in the structural scaffolds, independent of mechanical loading, with non-structural hydrogel constructs composed of the same alginate hydrogel but without the structural scaffold support,

2. Methods

2.1. Scaffold production

We evaluated two bone tissue-engineering scaffolds selected for their microstructural, mechanical, and functional properties (Fig. 1B). First, mechanically competent, structural scaffolds (PLDL) were fabricated through amorphous co-polymerization of poly(L-lactide) and poly(DL-lactide) with an L:DL ratio of 70:30 (PLDL; Purac America). PLDL pellets were mixed with 10% tricalcium phosphate particles (<200 nm diameter; Sigma Aldrich) and 30% azodicarbonamide (azo; Sigma Aldrich) as a heat-activated porogen. Porous scaffolds with combined longitudinal and random interconnected porosity were created, as described previously (Lin et al., 2003; Oest et al., 2007), through layered deposition of PLDL-

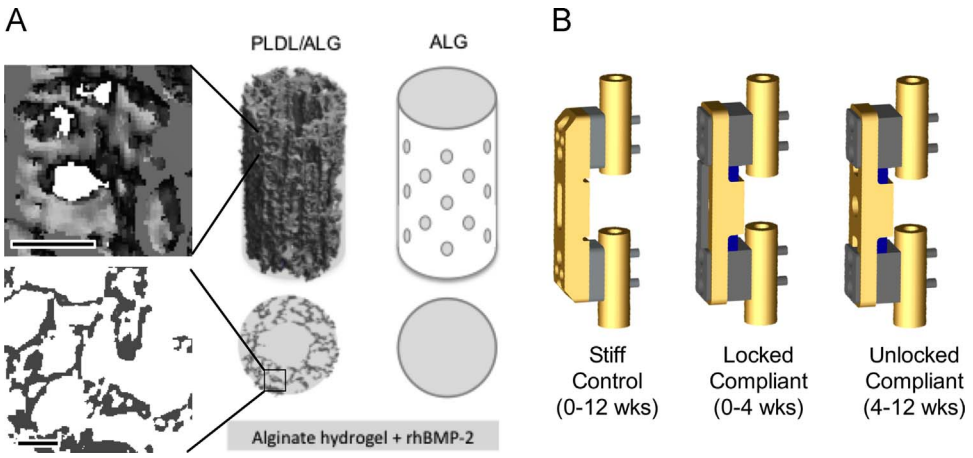

Fig. 1 – Tissue engineering constructs and stiff and compliant fixation plate configurations. (A) Structural PLDL/ALG scaffolds featured both random and axially-oriented porosity and 1.5 mm central core filled with RGD-functionalized alginate hydrogel containing rhBMP-2, while non-structural ALG constructs featured RGD-alginate and rhBMP-2, contained within a flexible perforated nanofiber mesh tube. Magnified images at left show porous scaffold architecture. Scale bars: 0.5 mm. In the ALG image at right, the alginate hydrogel is indicated in gray, while the perforated nanofiber mesh tube is shown in white. (B) For *in vivo* mechanical loading, control limbs received stiff plates (left), while experimental limbs received compliant plates initially implanted in the locked configuration for 4 weeks (center) and were unlocked at week 4 through week 12 (right).

azo on removable longitudinal fibers followed by rapid porogen decomposition at 260 °C (Lin et al., 2003). Cylindrical PLDL scaffolds were fabricated with 4 mm outer diameter and cut to 8 mm length, followed by punch removal of a 1.5 mm diameter core (Fig. 1A, left). Tricalcium phosphate particles were included to enhance cell adhesion and osteoconductivity of the PLDL scaffolds, and to buffer potential acidic degradation products of PLDL (Agrawal and Athanasiou, 1997; Lin et al., 2003; Oest et al., 2007). The pores and inner core of each scaffold was infused with alginate hydrogel, described below, to create composite PLDL/ALG constructs.

Second, non-structural hydrogel constructs (ALG) were fabricated using alginate hydrogel contained in electrospun nanofiber mesh tubes (Fig. 1A, right). Briefly, 5 Mrad-irradiated, Arg-Gly-Asp (RGD)-functionalized alginate polysaccharide chains were reconstituted to final concentration of 2% w/v and cross-linked with 0.21 g/ml calcium sulfate (Sigma Aldrich) at a ratio of 25:1 by volume (Alsberg et al., 2001). Alginate hydrogels were injected in situ into electrospun poly(ε-caprolactone) (PCL) nanofiber mesh tubes, which contained the hydrogel in the defect but did not provide axial structural support, as described previously (Boerckel et al., 2011a; Kolambkar et al., 2011a, 2011b). Briefly, PCL pellets (Sigma Aldrich) were dissolved in a 90:10 v/v solution of hexaflouoropropanol:dimethyl formamide, and electrospun onto a static collector plate at a distance of 20 cm with a voltage potential of ~20 kV, resulting in a ~3 μm-thick mesh of randomly-oriented nanofibers.

In both scaffold systems, sustained delivery of recombinant human BMP-2 (R&D Systems) was achieved through release from alginate hydrogel (Boerckel et al., 2011a). In the structural PLDL scaffolds, the pores and core regions were infused with alginate gel, while in the non-structural ALG constructs, crosslinked alginate was injected into non-structural nanofiber mesh tubes to contain the hydrogel in the defect (Boerckel et al., 2011a; Kolambkar et al., 2011b). These alginate hydrogels, formed though ionic crosslinking of alginate polysaccharides, exhibit shear-reversible gelation, enabling injection (Park et al., 2009). Samples in the alginate hydrogel group have been previously described in the dose-response study (Boerckel et al., 2011a) and analysis was expanded to enable comparison.

2.2. *Scaffold characterization*

To evaluate the structural characteristics and mechanical behavior of the PLDL scaffolds, scaffolds were evaluated by microCT imaging (microCT40, Scanco Medical) prior to and following 8 week dynamic incubation in basal cell culture medium at 37 °C *in vitro* to simulate effects of hydrolytic degradation *in vivo* ($N=6$ per group). Samples were scanned at 21 μm resolution at a voltage of 55 kVp and 109 μA. A global threshold was applied to segment scaffold material, and applied consistently across samples. Porosity was defined as 1-SV/TV, where SV is the scaffold volume and TV is the total volume enclosed by the scaffold, exclusive of the central cored region. Separate samples were tested in unconfined axial compression between flat plates to failure at 0.1 mm/s without and after *in vitro* degradation ($N=6$ per group). The effective modulus for each sample was computed as the slope from a linear regression of the engineering stress (defined as current force divided by microCT-derived average cross-sectional referential area) vs. linearized strain curve within the linear range (Fig. 2). The yield stress and strain were defined using the 0.2% offset approach. The ultimate stress was the maximum stress reached in the course of the test.

2.3. *Surgical procedure and experimental design*

Bilateral, critically-sized (8 mm) segmental defects were surgically created in femora of 13 week-old SASCO Sprague

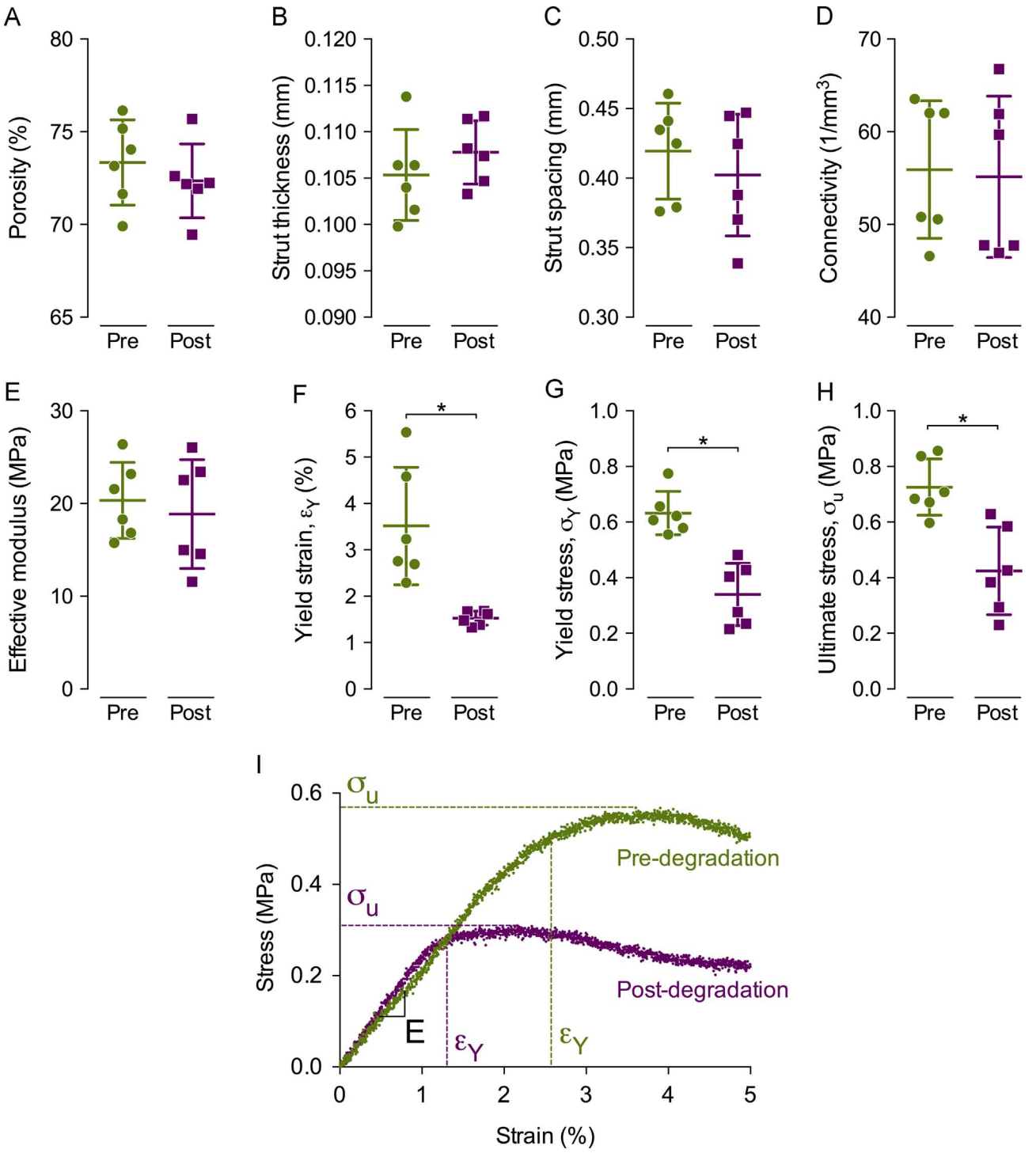

Fig. 2 – Structural and mechanical properties of PLDL scaffolds prior to and after eight weeks dynamic culture for degradation in vitro. Degradation had no effect on structural morphology, as measured by porosity (A), strut thickness (B), strut spacing (C), or connectivity (D) and did not alter the effective compressive modulus (E), but significantly reduced 0.2% offset yield strain (F) and stress (G) and ultimate stress (H). Representative stress-strain curves for scaffolds pre- and post-degradation (I) illustrate mechanical property changes. All data points plotted with mean ± s.d. * $p<0.05$, unpaired Student's t-test. $N=6$ per group.

Dawley rats, as previously described (Boerckel et al., 2011a, 2009; Oest et al., 2007). Prior to creation of the defect, limbs were stabilized by two types of custom fixation plates, described below, and implanted with two types of scaffolds containing rhBMP-2. The experimental design featured two studies, the first evaluating the influence of *in vivo* mechanical loading on large bone defect regeneration in the presence of a structural load-bearing scaffold, and the second

comparing regeneration in the structural scaffolds with regeneration in non-structural hydrogel constructs, without mechanical loading ($N=9$–10 per group). Post-surgery, animals were given subcutaneous injections of buprenorphine every 8 h for three days. All procedures were approved by the Institutional Animal Care and Use Committees (IACUC) of the University of Notre Dame (protocol #14-05-1778) and the Georgia Institute of Technology (protocol #A08032).

2.4. Fixation plates

To modulate the *in vivo* mechanical loading conditions, limbs were stabilized using custom internal fixation plates capable of modulating ambulatory load transfer, enabling two levels of *in vivo* loading, as characterized previously (Boerckel et al., 2009). Control limbs were stabilized by stiff plates (Fig. 1B, left) that allowed minimal transfer of axial, bending, or torsional loads (Boerckel et al., 2009). Experimental limbs received implantation of compliant fixation plates, which were initially implanted in the locked configuration (Fig. 1B, middle), preventing loading, but were unlocked at week 4 (Fig. 1B, right), allowing delayed axial load transfer, but maintaining a high stiffness to bending and torsional loads. $N=9$–10 per group. Fixation plate mechanical behavior is controlled by plate geometry as well as composition, with compliance conferred by deformability against integrated elastomers (shown in Fig. 1B in blue). The stiff fixation plates featured an axial stiffness of 214 N/mm, while the stiffness of the unlocked compliant plates was ~8.4 N/mm (Boerckel et al., 2009).

2.5. Radiographs and MicroCT

Two-dimensional radiographs (Faxitron MX-20 Digital, Faxitron X-ray Corp.) were taken at 2, 4, 8, and 12 weeks post-surgery. Three blinded observers evaluated the bridging rate as a binary score, determined by the number of samples at each time point featuring continuous bone connectivity across the defect in standardized orientation X-ray images. Results were verified using post-mortem quantification of bone formation and morphology was evaluated by microCT (microCT40, Scanco Medical) at 21.0 μm voxel size at a voltage of 55 kVp and a current of 109 μA. Bone tissue was segmented by application of a global threshold corresponding to 386 mg hydroxyapatite/cm^3, and a low-pass Gaussian filter (sigma: 0.8, support: 1) was used to suppress noise.

To quantitatively assess bone distribution, bone volumes were re-evaluated using a region of interest analysis, featuring three regions of interest (Fig. 5A). The 1.5 mm diameter core and cortex regions of interest coincided with the hollow core and porous structure regions of the PLDL scaffolds, respectively (cf. Fig. 1B). The cortex region was contained by a 4 mm diameter circle, centered on the defect region, with the 1.5 mm core removed. The radiodensity of the tricalcium phosphate particles within the PLDL scaffolds was indistinguishable from that of physiologic mineral, and was not removed from these groups since the degree of degradation and release was unknown in vivo; however, the total mineral volume represented by the tricalcium phosphate particles prior to any degradation was no greater than 2.3 mm^3, contributed exclusively in the cortex region. The ectopic region included any bone formation outside the outer diameter of the scaffold/defect. In the second study, post-mortem scans of ALG samples from a prior study (Boerckel et al., 2011a), which had previously been quantified only *in vivo*, precluding comparative analysis, were evaluated simultaneously with limbs receiving PLDL/ALG scaffolds, $N=8$–9 per group.

2.6. Mechanical testing

Mechanical function was evaluated in torsion to failure as described previously (Oest et al., 2007). Briefly, limbs were potted in low-melting temperature ($T_m=70$ °C) Wood's metal, and tested in torsion to failure at a rate of 3.0°/min. Torsional stiffness and ultimate torque were quantified. $N=8$–9 per group.

2.7. Histology

One representative sample per group was selected based on average microCT-quantified bone volume for qualitative histology at week 12. Limbs were decalcified for 14 days in a formic acid-based decalcifier containing 10% neutral buffered formalin (Cal-ExII, Fisher Scientific), or 0.25 M ethylenediaminetetraacetic acid (EDTA, Fisher Scientific) at pH 7.4, embedded in paraffin, sectioned to 4 μm in the sagittal plane, and stained with Haematoxylin and Eosin (H&E) and Safranin-O/Fast Green (Saf-O).

2.8. ELISA

BMP-2 release kinetics from ALG and PLDL/ALG scaffolds were evaluated by enzyme-linked immunosorbent assay (ELISA) *in vitro*. Scaffolds from each group ($N=3$ per group) were loaded with 500 ng rhBMP-2 per scaffold, and incubated in 37 °C PBS for 21 days. Supernatant (1 ml) was collected and replaced at 1, 2, 4, 7, 10, 14, and 21 days, and frozen for simultaneous analysis. The BMP-2 amount was selected to facilitate detection within the linear range of the ELISA assay for the given supernatant volume. At day 21, the alginate in each group was dissolved by incubation in 2% (w/v) sodium citrate. BMP-2 concentration in the collected buffer at each time point and in the sodium citrate solutions were assessed using an ELISA kit (R&D Systems) according to manufacturer instructions.

2.9. Statistical analysis

Summary statistics are presented as mean ± standard deviation or median with boxes indicating interquartile range and whiskers at 5th and 95th percentiles, as indicated. Multiple group comparisons were analyzed by analysis of variance (ANOVA), with pairwise post-hoc comparisons by Tukey's multiple comparisons test. Comparisons between two groups were assessed using unpaired, two-tailed Student's *t*-tests. Normality and homoscedasticity were verified by D'Agostino–Pearson omnibus normality test and Brown–Forsythe tests, respectively. Bridging trends within groups were assessed using the Chi square test for trend, with comparisons between groups by Chi square test, with Bonferroni

corrections for multiple comparisons (MacDonald and Gardner, 2000).

3. Results

3.1. *Part 1: Effects of mechanical loading on BMP-2-mediated bone regeneration in structural PLDL/ALG scaffolds*

First, we evaluated the effects of *in vivo* mechanical loading on large bone defect regeneration in structural, load-bearing scaffolds. Structural PLDL scaffolds were infused, including the cored center region, with alginate hydrogel containing a total of three micrograms rhBMP-2, and implanted in bone defects stabilized by either stiff fixation plates that allowed minimal load sharing, or axially compliant fixation plates, initially implanted in a locked configuration to prevent load transfer, but unlocked at week 4 to initiate ambulatory load transfer. We assessed bone regeneration over 12 weeks, allowing 8 weeks of loading in the compliant plate group.

3.2. *Structural PLDL scaffold properties*

MicroCT scanning and mechanical testing were performed to characterize the architectural and mechanical properties of the PLDL scaffolds, prior to and after *in vitro* hydrolytic degradation for 8 weeks. Scaffolds had initial porosity of 73.3±2.3% and effective modulus of 20.3±4.1 MPa. Following 8 weeks *in vitro* degradation, there were no gross morphometric changes in either scaffold architecture (Fig. 2A-D) or elastic behavior (Fig. 2E); however, in vitro degradation significantly altered the failure properties, reducing yield strain by 57% (Fig. 2F), yield stress by 46% (Fig. 2G) and ultimate stress by 41% (Fig. 2H). These changes in material properties are illustrated in representative stress-strain curves for PLDL samples pre- and post-degradation (Fig. 2I).

3.3. *Radiographic bridging*

Radiographic assessment of bony bridging at weeks 4, 8, and 12 found no significant differences in rate or incidence of bridging between loading conditions at any time point (Fig. 3A and B). At week 4, the time point of compliant plate actuation, the stiff and compliant plate groups achieved bridging incidence of 30% and 10%, respectively, but were not statistically distinguishable. Both groups plateaued at a bridging incidence of 40% by weeks 8–12.

3.4. *Bone formation*

Post mortem microCT evaluation of bone formation revealed no differences between stiff or delayed loading groups for total bone volume within the defect ($p=0.88$, $\beta=0.94$; Fig. 3C and D). In addition, a similar pattern of bone deposition was observed for the two groups, with bone formation concentrated in the core region and around the periphery of the scaffold (Fig. 3D). To quantify these distributions, a region of interest analysis was conducted, but there were no significant

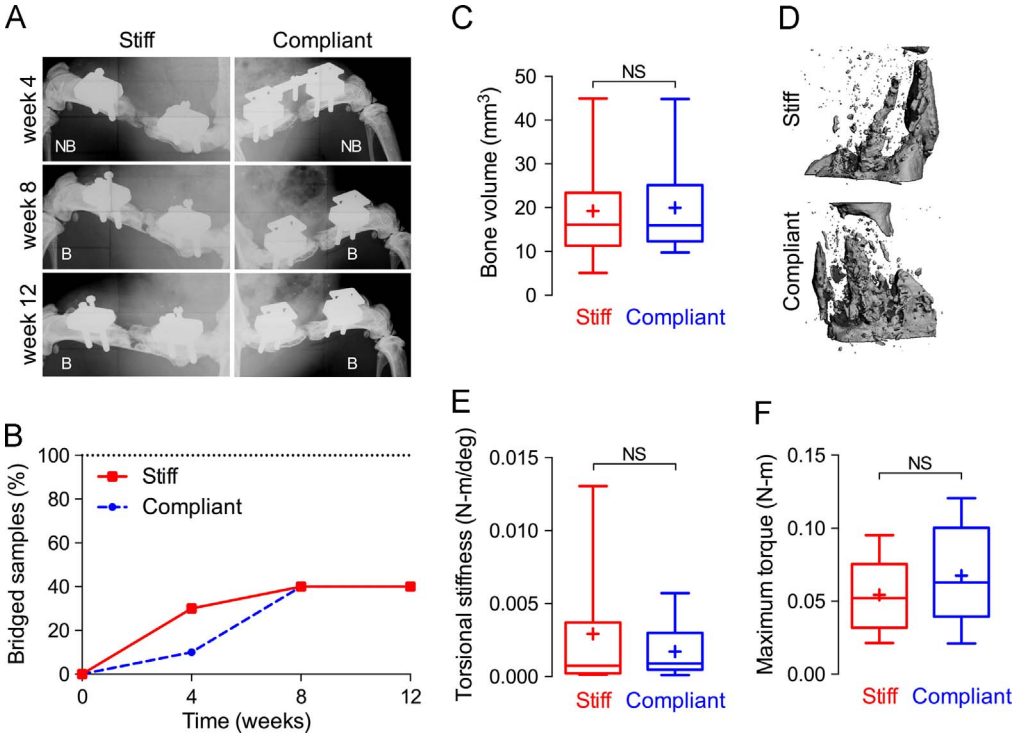

Fig. 3 – Effects of mechanical loading on bone regeneration in structural PLDL/ALG scaffolds. Delayed *in vivo* loading had no effect on defect bridging (A,B), bone formation (C,D), or torsional mechanical properties at week 12 (E,F). Binary bridging scores (bridged – B or not bridged – NB) are indicated on representative radiographs. Box plots show 25th, and 75th percentiles, with whiskers at 5th and 95th percentiles, respectively. Mean values indicated by +. NS: $p>0.05$, Student's *t*-test. $N=9$–10 per group.

differences in new bone distribution between groups (Supplementary Fig. 1).

3.5. Biomechanics

Torsion testing of excised limbs to failure revealed no significant differences in torsional stiffness or maximum torque to failure between stiff and compliant plate groups, indicating no differences in functional regeneration ($p=0.34$, $\beta=0.83$ and $p=0.54$, $\beta=0.75$, respectively; Fig. 3E and F).

3.6. Part 2: Influence of structural scaffold on bone regeneration induced by alginate-mediated BMP-2 delivery

To evaluate the effect of the structural scaffold on bone regeneration without mechanical loading, regeneration in the structural scaffolds was compared to non-structural alginate constructs (ALG) in which the alginate hydrogel was contained in the defect by a perforated, non-structural nanofiber mesh, described previously (Boerckel et al., 2011a; Kolambkar et al., 2011b). The samples from the 2.5 μg rhBMP-2 group in a prior dose-response study for the ALG group (Boerckel et al., 2011a) were re-evaluated for comparison with the PLDL/ALG samples from Part 1.

3.7. Radiographic bridging

PLDL/ALG constructs had a significantly lower bridging rate compared to ALG at weeks 8 and 12 ($p<0.05$, Chi square test), with the ALG group exhibiting a significantly positive bridging rate over time ($p<0.001$, Chi square test for trend) to a maximum of 80% at week 12 (Fig. 4A and B).

3.8. Bone formation

Post-mortem microCT evaluation revealed a significant 77% lower bone volume in the PLDL/ALG group compared to ALG (Fig. 4C and D). When observing representative images, bone formation in ALG samples appeared more evenly distributed

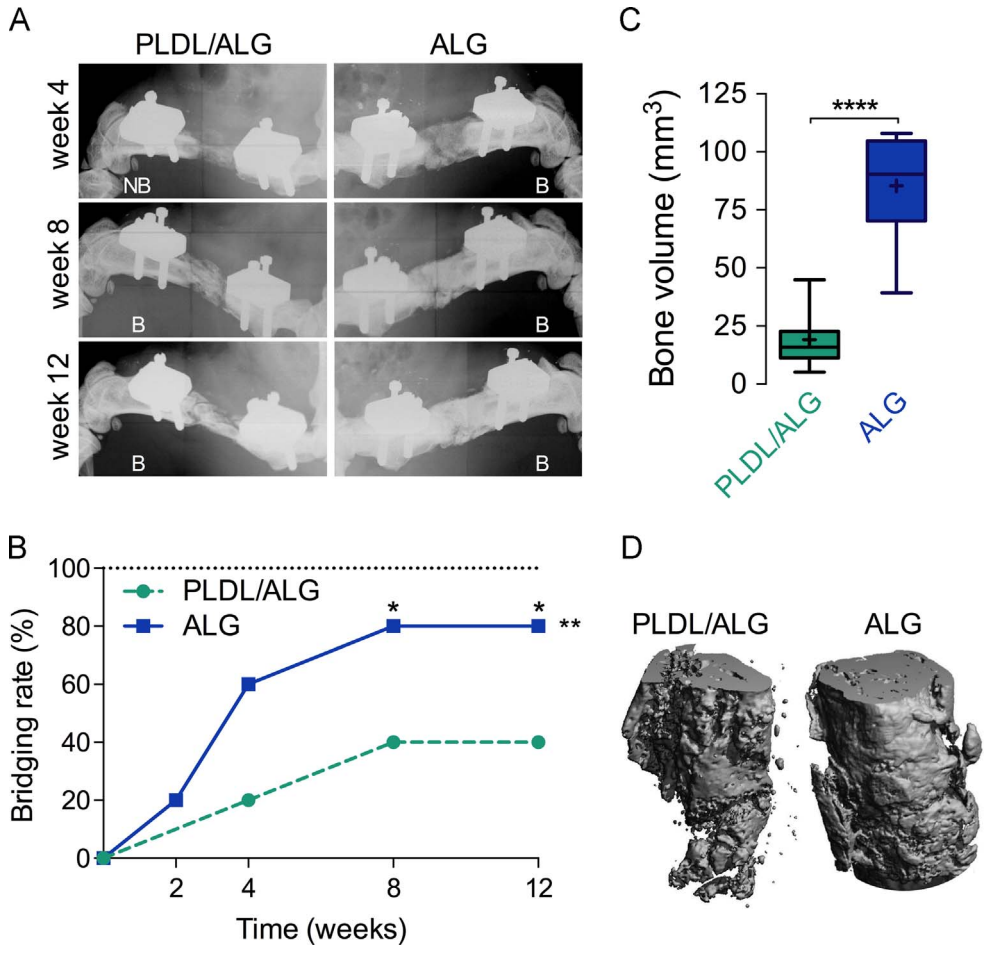

Fig. 4 – Comparison of bone formation in PLDL/ALG and ALG constructs independent of mechanical loading. ALG constructs exhibited a significantly increasing trend in bridging rate over time (Chi Square test for trend, $p<0.01$), while PLDL/ALG did not ($p>0.73$) (A). Comparison of bridging rates between groups at week 12 was statistically significant ($p<0.05$). Bridging rates were evaluated from 2D radiographs, shown at weeks 4, 8, and 12 with bridging scores (bridged – B or not bridged – NB) as indicated (B). ALG constructs had significantly greater bone volume (C), illustrated by high-resolution post-mortem microCT reconstructions (D). Box plots show 25th, and 75th percentiles, with whiskers at 5th and 95th percentiles, respectively. Mean values indicated by +. $^{****}p<0.0001$, unpaired Student's t-test. $N=6$–19 per group.

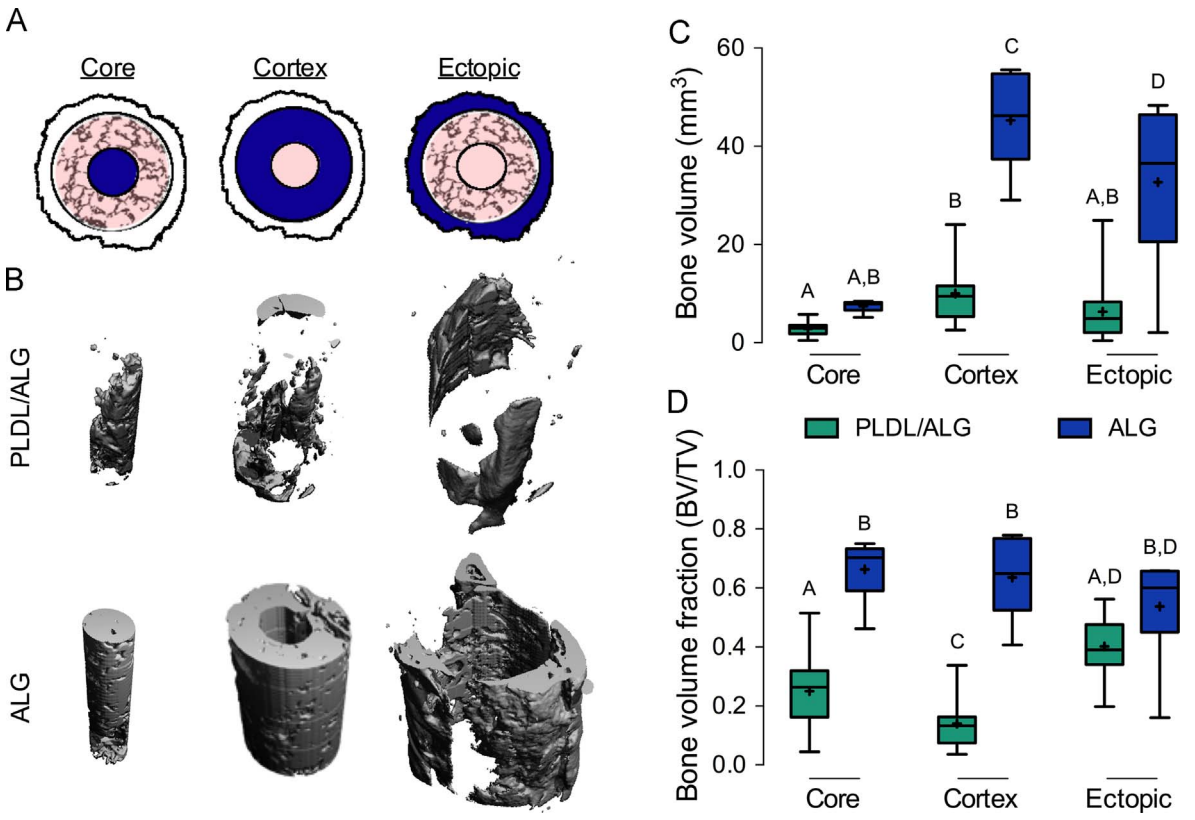

Fig. 5 – Region of interest analysis of bone distribution. Bone formation was evaluated in three regions of interest defined by the inner core region, the cortex region, which was coincident with the annular PLDL scaffold, and the ectopic region, respectively (A). Bone formation in the PLDL/ALG and ALG groups was evaluated in each region (B) and quantified for total bone volume (C) and bone volume fraction, BV/TV (D). Comparison of BV and BV/TV among and between groups was performed by two-way ANOVA with Tukey's multiple comparisons test. Box plots show 25th, and 75th percentiles, with whiskers at 5th and 95th percentiles, respectively. Mean values indicated by +. Letters shared in common between or among groups indicate no significant difference. $N=6$–19 per group.

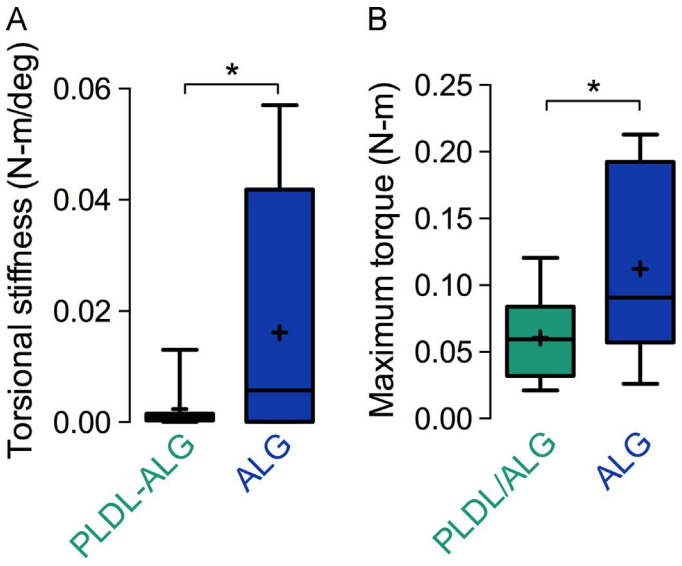

Fig. 6 – Functional regeneration assessed by mechanical testing in torsion to failure. Torsional stiffness (A) and maximum torque at failure (B) were significantly greater in the ALG group (*$p<0.05$, unpaired Student's t-test), though both were lower than the properties of intact limbs (0.030 ± 0.001 N-m/deg and 0.31 ± 002 N-m, respectively) (Boerckel et al., 2009). Box plots show 25th, and 75th percentiles, with whiskers at 5th and 95th percentiles, respectively. Mean values indicated by +. $N=8$–19 per group.

throughout the defect compared to the PLDL/ALG group (Fig. 4D).

3.9. Bone distribution

Volumetric region of interest analysis (Fig. 5A) indicated the ALG group exhibited a significantly higher bone volume in both the ectopic and cortex regions, but not in the core region compared to the PLDL/ALG group (Fig. 5B and C). To enable direct comparison of bone distribution within each scaffold type, the bone volume fraction (BV/TV) was computed in each region (Fig. 5D).There were no significant differences in BV/TV between regions for ALG scaffolds, while PLDL/ALG scaffolds had significantly higher BV/TV in the ectopic and core regions compared to the cortex, in which the scaffold itself was located. In addition, bone volume fraction was lower in the PLDL/ALG group in all regions except the ectopic region.

3.10. Biomechanics

Post-mortem mechanical testing revealed a significantly greater torsional stiffness and maximum torque at failure in the ALG group compared to PLDL/ALG (Fig. 6).

3.11. Histology

Histological evaluation of tissue formation was evaluated by Haematoxylin and Eosin (H&E) and Safranin-O/Fast Green staining at week 12 post surgery. Bone formation was present throughout the defect in the ALG group, forming appositionally on and around particles of alginate hydrogel (Fig. 7, Supplementary Fig. 2). In the PLDL/ALG group, bone formation was predominantly localized to the core and ectopic regions, with significant remaining PLDL scaffold evident in the cortex region (Fig. 7, Supplementary Fig. 2). Interestingly, substantial amounts of cartilage formation (c) were present in the PLDL/ALG group, frequently adjacent to the scaffold struts, indicated by presence of chondrocytes and staining for negatively charged glycosaminoglycans by Safranin-O. Positive control slides from distal femur growth plate are shown in Supplementary Fig. 3. Both groups exhibited residual alginate in the defect at week 12 post-surgery.

3.12. BMP-2 release kinetics

In vitro BMP-2 release kinetics were similar for both groups, exhibiting a total release of ~40ng over 28 days with a half-life of release of 6.8±2.8 and 3.9±2.1 days (mean±std. dev.) for ALG and PLDL/ALG groups, respectively (Fig. 8). Neither release rate nor total release was significantly different ($p>0.05$) between groups. The amount of BMP-2 left in each scaffold at day 28 was 41.4±21.9 and 71.1±20.0 ng (mean±std. dev.) in ALG and PLDL/ALG groups, respectively. Differences in remaining protein were not significant (unpaired Student's *t*-test, $p>0.05$).

4. Discussion

Tissue engineering scaffolds for bone regeneration are frequently designed to match, as closely as possible, the mechanical properties of the native tissue (Butler et al., 2009; Tang et al., 2016). Particularly in bone, structural scaffolds are attractive for load-bearing bone defects to

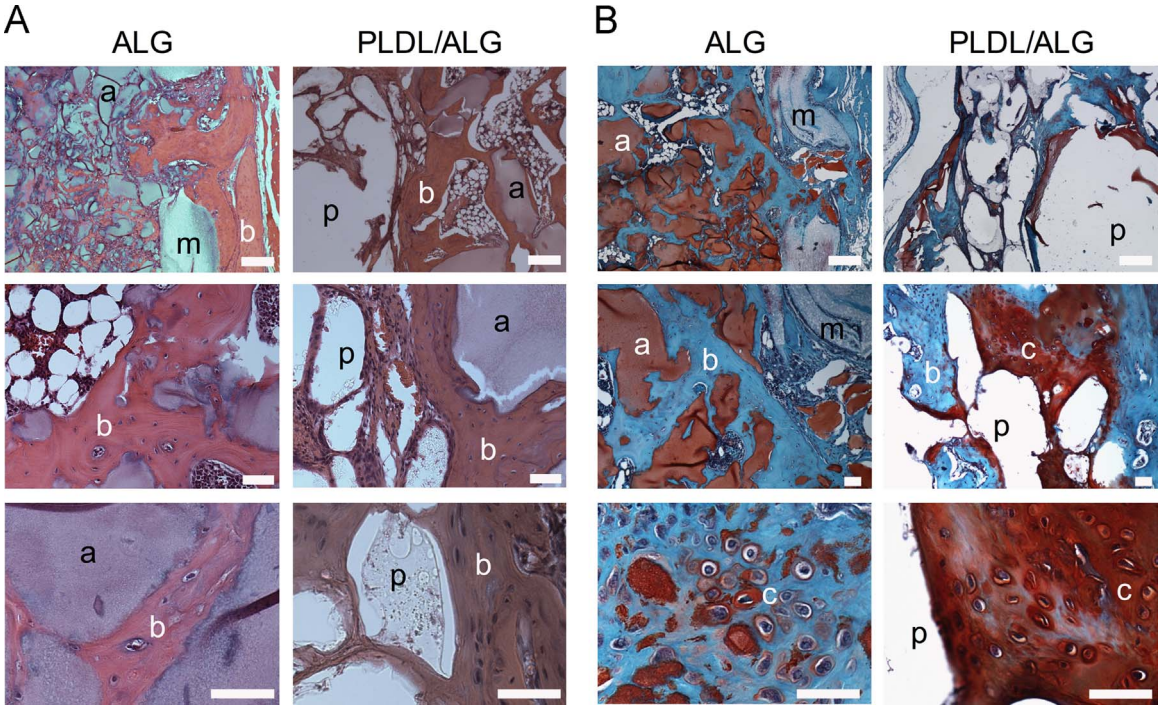

Fig. 7 – Histological comparison PLDL/ALG and ALG-mediated regeneration at week 12. Haematoxylin and Eosin (H&E) (A) and Safranin-O/Fast Green (B) staining showing bone formation (b), cartilage formation (c), alginate hydrogel (a), PLDL scaffold (p), nanofiber mesh (m). Scale bars: top row – 250 μm, all others – 50 μm.

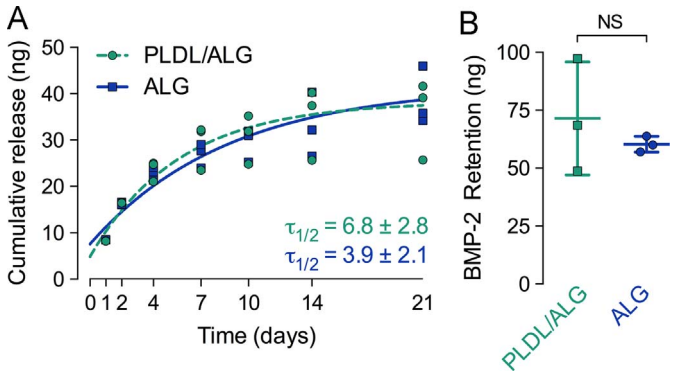

Fig. 8 – BMP-2 release *in vitro*. Cumulative release data (A) were fit to a one-phase exponential curve, and the half-life of protein release was calculated: 6.8±2.8 and 3.9±2.1 days for ALG and PLDL/ALG groups, respectively. The remaining BMP-2 retained in the constructs was evaluated after alginate dissolution in sodium citrate at day 21. (B) There were no differences in release kinetics, total release, or protein retention between groups (Student's *t*-test, $p>0.05$). Error bars in (A) indicate standard deviations. All data points shown with nonlinear regression to exponential decay function (A) or mean±s.d. (B). $N=3$ per group.

enable load sharing between the construct and fixation hardware to promote functional use as soon as possible. However, if the fixation system is sufficiently durable to withstand *in vivo* loading, this constraint may not be necessary, allowing use of either structural or non-structural materials as graft substitutes. This presents the question of which are preferable for mechanical load-induced bone regeneration: structural scaffolds that can bear physiologic loads or non-structural scaffolds that enable rapid replacement with newly-formed tissue.

This study tested the hypothesis that mechanical loading would enhance bone regeneration in the presence of a structural, load-bearing scaffold, similar to our prior observations on mechanical regulation of bone regeneration in non-load-bearing hydrogel constructs (Boerckel et al., 2012, 2011b, 2009). In this experiment, we replicated the loading time-course that had a positive effect on bone regeneration in the hydrogel system (Boerckel et al., 2011b): delayed loading with compliant plates unlocked at week 4 post-implantation. Contrary to the hypothesis, delayed *in vivo* mechanical loading had no effect on bone formation, distribution, or functional regeneration at week 12 in the presence of a structural scaffold. Slight differences in bridging incidence were apparent at week 4 but these were not statistically significant and fell within the range of experimental variability typical of this model (Boerckel et al., 2011a).

One rationale for using load-bearing scaffolds in combination with mechanical loading is that the scaffolds may promote transfer of stimulatory loads to in-growing bone prior to complete defect bridging. However, as loading was not effective under these conditions, the high stiffness of the scaffold may have contributed a stress-shielding effect, sheltering the ingrowing tissue from stimulation. This is supported by the observation that the elastic properties of the scaffolds within the range of expected loads *in vivo* did not change by *in vitro* degradation, suggesting the scaffolds maintained mechanical integrity and load-bearing, and were not functionally replaced with new bone. The axial load amplitude *in vivo* in the compliant plate group was previously calculated at approximately 3N (Boerckel et al., 2012), which corresponds to a maximum effective interfragmentary strain amplitude of 0.6% in the scaffolds, assuming no tissue ingrowth, indicating the scaffolds remained within the elastic range *in vivo*.

A potential limitation of the bilateral defect model for studies of the influence of mechanics is the possibility of differential weight-bearing between limbs since this is essential for ambulatory mechanical stimulation in this model. While we did not directly measure differential weight bearing in this experiment, several lines of evidence from our prior and ongoing studies suggest that bilateral weight bearing is uniform and sufficient for mechanical stimulation (Boerckel et al., 2012; Uhrig et al., 2014; Willett et al., 2013). First, we previously performed a quantitative dynamic gait analysis on animals receiving unilateral defects and found no significant difference in either duty cycle or paw print area compared to contralateral unoperated limbs, suggesting that the bone defect surgery and fixation do not induce preferential limb unloading (Uhrig et al., 2014; Willett et al., 2013). Second, we have observed consistent enhancement of bone regeneration by delayed mechanical loading in multiple studies (Boerckel et al., 2012, 2011b). Finally, recent data on paired stiff-compliant or compliant-compliant limbs do not exhibit differential responses (data not shown).

In the second part of the study, we compared bone regeneration in the structural scaffolds with the non-structural hydrogel constructs (Boerckel et al., 2012, 2011a, 2011b), independent of mechanical loading. In this analysis, the presence of the structural scaffold significantly reduced bone formation and functional mechanical properties and altered the distribution of new bone in the defect. Specifically, bone formation was reduced in the core and cortex regions, but was not significantly different in the ectopic region. Bone formed least in the cortex region, which was coincident with the annular scaffold, and the difference in bone volume fraction compared to the ectopic region (0.28) was identical to the average post-degradation volume fraction of that region which contained the scaffold (*i.e.* 72% scaffold

porosity). Consistently, while the core region exhibited lower bone volume than the cortex region, the core also had a significantly higher volume fraction than the cortex region. Compared to the ALG group, however, the bone volume fraction in both the core and cortex regions were significantly lower than just the amount of space occupied by the scaffold. Taken together, these data indicate that the scaffold itself reduced bone formation in the defect by occupying potential space and impeding bone growth into the central core from the periphery. A limitation of this analysis is that the BMP-2 dose delivered in the PLDL/ALG group was 3.0 μg, while it was 2.5 μg in the ALG group. However, the bone formation response was significantly greater in the ALG group, which received the lower dose. Further, these doses are in the middle of the range of doses we have previously evaluated, which exhibited a clear positive dose response between 0 and 5 μg BMP-2 (Boerckel et al., 2011a), and similar spatial distribution patterns at both 2.5 μg (Fig. 5) and 5 μg BMP-2 (Kolambkar et al., 2011a). Therefore, since we would have expected an even greater response due to dose in the PLDL/ALG group, this further supports the stated conclusions. The sub-saturation dose of BMP-2 was selected to induce bone regeneration, but enable evaluation of potential regeneration enhancement by mechanical loading, as described previously (Boerckel et al., 2011b).

In addition to stress shielding and structural interference, it is possible that PLDL scaffold degradation influenced bone formation. The poly(lactic acid) polymers are known to produce acidic byproducts during hydrolytic degradation, which may adversely affect osteogenesis through an enhanced inflammatory response (Solheim et al., 2000). However, the slow degradation rate of the PLDL co-polymer formulation selected has been shown to limit local acidic concentration (Kellomäki et al., 2000; Leiggener et al., 2006; Solheim et al., 2000), and low w/v tricalcium phosphate microparticles were included to buffer the degradation products (Agrawal and Athanasiou, 1997). The poly(lactic acid) polymers are use extensively as delivery vehicles for growth factors, including BMP-2, and have been shown maintain BMP-2 activity and osteoinductivity (Kaito et al., 2005; Wildemann et al., 2004) and promote new bone growth (Kaito et al., 2005; Meinig et al., 1997). In the present study, histological evaluation revealed cartilage formation adjacent to PLDL scaffold struts, which were not present in the ALG group, suggesting a potential effect of the scaffold on local tissue hypoxia, though comparison of erythrocyte-positive blood vessels in H&E-stained sections between groups were not apparent (Supplementary Fig. 4).

Structural scaffold inclusion did not affect protein delivery kinetics *in vitro*. Though *in vitro* and *in vivo* release rates are likely to differ, and we did not evaluate the effects of mechanical loading on protein release (Lee et al., 2000), this data suggests that the effect of the scaffold on load-mediated bone formation was primarily through scaffold structural properties and not through interference of inductive protein presentation. As is frequently observed with the supernatant ELISA assay, the total protein release measured did not add up to the amount initially loaded as some is left in the scaffold (measured at 10–15% in both groups), some is degraded and lost prior to detection, and some may not be detected by the assay. Together, with differences between *in vitro* conditions and those *in vivo*, these data suggest the *in vivo* release kinetics may be underestimated by the *in vitro* assay. Regardless, the differences between groups can be compared *in vitro*.

The observations that intrinsic matrix mechanical properties can alter progenitor cell recruitment and fate independent of biochemical cues (Engler et al., 2006) have heightened attention on scaffold mechanical properties, not only for mechanical similarity (Butler et al., 2000), but also of the microenvironmental mechanical signals presented to delivered or endogenous cells (Chaudhuri et al., 2015; Huebsch et al., 2015). For example, the concept of durotaxis, or cellular motility driven by gradients in matrix rigidity, has been proposed as an explanation for the ability of MSCs to home to sites of injury (Discher et al., 2009). Similarly, MSC lineage specification may be controlled by matrix rigidity, with preferential differentiation toward adipogenic and osteogenic lineages on soft and stiff substrates, respectively (Engler et al., 2006). Recently, Huebsch et al. demonstrated that alginate matrix rigidity controlled bone regeneration *in vivo*, with an optimal elasticity of approximately 60 kPa (bulk modulus) (Huebsch et al., 2015). Thus, seeding progenitor cells onto the scaffold prior to implantation may enable local transmission of mechanical signals throughout the defect and enhance mechanosensitivity; however, the length scales governing cellular mechanotransduction differ from those of bulk properties, and elucidating the direct influence of heterogeneous scaffold properties and architecture on endogenous and exogenously-supplied cell behavior will require continued research.

Given the longitudinal orientation of the porosity and high stiffness of the PLDL scaffolds, we initially hypothesized that these would enhance cellular recruitment and osteogenic differentiation compared to the relatively soft hydrogel constructs. However, migration through the interstitial alginate, functionalized with RGD peptides, appeared to be the primary means of cellular infiltration, which may have minimized differences in mechanical signals between groups. Further, the primarily longitudinal orientation of the scaffold porosity may also have reduced the ability of cells to migrate in from the surrounding tissues. This is particularly critical for neovascularization, which we found previously is controlled by mechanical loading, and invades primarily radially from the surrounding muscle (Boerckel et al., 2011b).

The optimal extrinsic mechanical conditions for large bone defect regeneration remain unknown, and both the delayed loading approach described here (Boerckel et al., 2012, 2011b, 2009), and a reverse dynamization approach in which moderate stiffness fixators were replaced by stiff fixators after two weeks (Glatt et al., 2012) have been shown to enhance regeneration. Consistent with the present observations, in each of these systems in which loading enhanced bone formation, BMP-2 was delivered in non-structural constructs (alginate or collagen sponge). In our previous study (Boerckel et al., 2011b), we found that large deformations associated with early loading inhibited neovascular ingrowth and bone formation; however, future studies will be required to test whether early loading of structural scaffolds would exhibit different behavior, as the scaffold could limit

interfragmentary strains in the early stages of healing. Similarly, while excessively stiff scaffolds may inhibit load-induced regeneration, scaffolds with moderate elastic moduli may instead facilitate mechanical stimulation through both intrinsic and extrinsic cues.

5. Conclusions

Collectively, these observations indicate that structural scaffolds can impede the beneficial effect of mechanical loading by stress shielding and inhibition of cellular infiltration and tissue ingrowth. This suggests that the common design constraint that tissue engineering scaffolds possess similar mechanical properties to the replaced tissue is not requisite for load-bearing tissues, given appropriate fixation conditions. These data instead emphasize the importance of recreating an adequate environment to enable cells to activate matrix production and achieve ultimate functional regeneration. Indeed, like early fracture healing, optimal matrix properties at the onset of tissue regeneration may be much lower than those of the fully regenerated tissue; however, further studies will be required to evaluate whether the stress-shielding effects of load-bearing scaffolds inhibit mechanical stimulation of bone regeneration regardless of scaffold composition.

Acknowledgments

This work was supported by grants from the Naughton Foundation (to JDB, AMM) and the Indiana Clinical and Translational Science Institute (ICTSI NIH/NCRR UL1TR001108 to JDB). The authors would like to thank Dr. Kenneth Dupont, and Dr. Yash Kolambkar for their assistance, and Dr. David Mooney for providing the RGD alginate.

Appendix A. Supporting information

Supplementary data associated with this article can be found in the online version at http://dx.doi.org/10.1016/j.jmbbm.2016.05.010.

REFERENCES

Agrawal, C.M., Athanasiou, K.A., 1997. Technique to control pH in vicinity of biodegrading PLA-PGA implants. J. Biomed. Mater. Res. 38, 105–114.

Alsberg, E., Anderson, K.W., Albeiruti, A., Franceschi, R.T., Mooney, D.J., 2001. Cell-interactive alginate hydrogels for bone tissue engineering. J. Dent. Res. 80, 2025–2029.

Bailey, J.L., Critser, P.J., Whittington, C., Kuske, J.L., Yoder, M.C., Voytik-Harbin, S.L., 2011. Collagen oligomers modulate physical and biological properties of three-dimensional self-assembled matrices. Biopolymers 95, 77–93.

Boerckel, J.D., Dupont, K.M., Kolambkar, Y.M., Lin, A.S.P., Guldberg, R.E., 2009. In vivo model for evaluating the effects of mechanical stimulation on tissue-engineered bone repair. J. Biomech. Eng. 131, 084502.

Boerckel, J.D., Kolambkar, Y.M., Dupont, K.M., Uhrig, B. a, Phelps, E. a, Stevens, H.Y., García, A.J., Guldberg, R.E., 2011a. Effects of protein dose and delivery system on BMP-mediated bone regeneration. Biomaterials 32, 5241–5251.

Boerckel, J.D., Kolambkar, Y.M., Stevens, H.Y., Lin, A.S.P., Dupont, K.M., Guldberg, R.E., 2012. Effects of in vivo mechanical loading on large bone defect regeneration. J. Orthop. Res. 30, 1067–1075.

Boerckel, J.D., Uhrig, B. a, Willett, N.J., Huebsch, N., Guldberg, R.E., 2011b. Mechanical regulation of vascular growth and tissue regeneration in vivo. Proc. Natl. Acad. Sci. USA 108, E674–E680.

Butler, D.L., Goldstein, S.A., Guilak, F., 2000. Functional tissue engineering: the role of biomechanics. J. Biomech. Eng. 122, 570–575.

Butler, D.L., Goldstein, S.A., Guldberg, R.E., Guo, X.E., Kamm, R., Laurencin, C.T., McIntire, L.V., Mow, V.C., Nerem, R.M., Sah, R. L., Soslowsky, L.J., Spilker, R.L., Tranquillo, R.T., 2009. The impact of biomechanics in tissue engineering and regenerative medicine. Tissue Eng. Part B. Rev. 15, 477–484.

Carter, D.R., Van der Meulen, M.C.H., Beaupré, G.S., 1996. Mechanical factors in bone growth and development. Bone 18, S5–S10.

Chaudhuri, O., Gu, L., Darnell, M., Klumpers, D., Bencherif, S.A., Weaver, J.C., Huebsch, N., Mooney, D.J., 2015. Substrate stress relaxation regulates cell spreading. Nat. Commun. 6, 6364.

Claes, L., Augat, P., Suger, G., Wilke, H., 1997. Influence of size and stability of the osteotomy gap on the success of fracture healing. J. Orthop. Res. 15, 577–584.

Claes, L., Wilke, H.J., Augat, P., Suger, G., Fleischman, W., 1994. The influence of fracture gap size and stability on bone healing. In: Transactions of the 40th An Nual Meeting Orthopaedic Research Society, New Orleans, LA. p. 203.

Claes, L.E., Heigele, C. a, Neidlinger-Wilke, C., Kaspar, D., Seidl, W., Margevicius, K.J., Augat, P., 1998. Effects of mechanical factors on the fracture healing process. Clin. Orthop. Relat Res 355S, S132–S147.

Claes, L.E., Heigele, C.A., 1999. Magnitudes of local stress and strain along bony surfaces predict the course and type of fracture healing. J. Biomech. 32, 255–266.

Discher, D.E., Mooney, D.J., Zandstra, P.W., 2009. Growth factors, matrices, and forces combine and control stem cells. Science 324, 1673–1677.

Duyck, J., Vandamme, K., 2014. The effect of loading on peri-implant bone: a critical review of the literature. J. Oral Rehabil. 41, 783–794.

Engler, A.J., Sen, S., Sweeney, H.L., Discher, D.E., 2006. Matrix elasticity directs stem cell lineage specification. Cell 126, 677–689.

Glatt, V., Miller, M., Ivkovic, A., Liu, F., Parry, N., Griffin, D., Vrahas, M., Evans, C., 2012. Improved healing of large segmental defects in the rat femur by reverse dynamization in the presence of bone morphogenetic protein-2. J. Bone Joint Surg. Am. 94, 2063–2073.

Gómez-Benito, M.J., García-Aznar, J.M., Kuiper, J.H., Doblaré, M., 2005. Influence of fracture gap size on the pattern of long bone healing: a computational study. J. Theor. Biol. 235, 105–119.

Goodship, A.E., Kenwright, J., 1985. The influence of induced micromovement upon the healing of experimental tibial fractures. J. Bone Joint Surg. Br. 67, 650–655.

Guldberg, R.E., Caldwell, N.J., Guo, X.E., Goulet, R.W., Hollister, S.J., Goldstein, S. a, 1997. Mechanical stimulation of tissue repair in the hydraulic bone chamber. J. Bone Miner. Res. 12, 1295–1302.

Huebsch, N., Lippens, E., Lee, K., Mehta, M., Koshy, S.T., Darnell, M.C., Desai, R.M., Madl, C.M., Xu, M., Zhao, X., Chaudhuri, O., Verbeke, C., Kim, W.S., Alim, K., Mammoto, A., Ingber, D.E., Duda, G.N., Mooney, D.J., 2015. Matrix elasticity of void-forming hydrogels controls transplanted-stem-cell-mediated bone formation. Nat. Mater. Epub ahead of print.

Jeon, O., Bouhadir, K.H., Mansour, J.M., Alsberg, E., 2009. Photocrosslinked alginate hydrogels with tunable biodegradation rates and mechanical properties. Biomaterials 30, 2724–2734.
Kaito, T., Myoui, A., Takaoka, K., Saito, N., Nishikawa, M., Tamai, N., Ohgushi, H., Yoshikawa, H., 2005. Potentiation of the activity of bone morphogenetic protein-2 in bone regeneration by a PLA-PEG/hydroxyapatite composite. Biomaterials 26, 73–79.
Keane, T.J., Badylak, S.F., 2014. Biomaterials for tissue engineering applications. Semin. Pediatr. Surg. 23, 112–118.
Kellomäki, M., Paasimaa, S., Törmälä, P., 2000. Pliable polylactide plates for guided bone regeneration: manufacturing and in vitro. Proc. Inst. Mech. Eng. H 214, 615–629.
Kenwright, J., Richardson, J.B., Goodship, A.E., Evans, M., Kelly, D. J., Spriggins, A.J., Newman, J.H., Burrough, S.J., Harris, J.D., Rowley, D.I., 1986. Effect of controlled axial micromovement on healing of tibial fractures. Lancet (London, England) 2, 1185–1187.
Kolambkar, Y.M., Boerckel, J.D., Dupont, K.M., Bajin, M., Huebsch, N., Mooney, D.J., Hutmacher, D.W., Guldberg, R.E., 2011a. Spatiotemporal delivery of bone morphogenetic protein enhances functional repair of segmental bone defects. Bone 49, 485–492.
Kolambkar, Y.M., Dupont, K.M., Boerckel, J.D., Huebsch, N., Mooney, D.J., Hutmacher, D.W., Guldberg, R.E., 2011b. An alginate-based hybrid system for growth factor delivery in the functional repair of large bone defects. Biomaterials 32, 65–74.
Kreger, S.T., Bell, B.J., Bailey, J., Stites, E., Kuske, J., Waisner, B., Voytik-Harbin, S.L., 2010. Polymerization and matrix physical properties as important design considerations for soluble collagen formulations. Biopolymers 93, 690–707.
Lacroix, D., Prendergast, P.J., 2002. A mechano-regulation model for tissue differentiation during fracture healing: analysis of gap size and loading. J. Biomech. 35, 1163–1171.
Lee, K.Y., Peters, M.C., Anderson, K.W., Mooney, D.J., 2000. Controlled growth factor release from synthetic extracellular matrices. Nature 408, 998–1000.
Leiggener, C.S., Curtis, R., Müller, A.A., Pfluger, D., Gogolewski, S., Rahn, B.A., 2006. Influence of copolymer composition of polylactide implants on cranial bone regeneration. Biomaterials 27, 202–207.
Lin, A.S.P., Barrows, T.H., Cartmell, S.H., Guldberg, R.E., 2003. Microarchitectural and mechanical characterization of oriented porous polymer scaffolds. Biomaterials 24, 481–489.
MacDonald, P.L., Gardner, R.C., 2000. Type I error rate comparisons of post hoc procedures for I j Chi-Square tables. Educ. Psychol. Meas. 60, 735–754.
Mason, B.N., Starchenko, A., Williams, R.M., Bonassar, L.J., Reinhart-King, C.A., 2013. Tuning three-dimensional collagen matrix stiffness independently of collagen concentration modulates endothelial cell behavior. Acta Biomater. 9, 4635–4644.
Matziolis, G., Tuischer, J., Kasper, G., Thompson, M., Bartmeyer, B., Krocker, D., Perka, C., Duda, G., 2006. Simulation of cell differentiation in fracture healing: mechanically loaded composite scaffolds in a novel bioreactor system. Tissue Eng. 12, 201–208.
Mauney, J.R., Sjostorm, S., Blumberg, J., Horan, R., O'Leary, J.P., Vunjak-Novakovic, G., Volloch, V., Kaplan, D.L., 2004. Mechanical stimulation promotes osteogenic differentiation of human bone marrow stromal cells on 3-D partially demineralized bone scaffolds in vitro. Calcif. Tissue Int. 74, 458–468.
Meinig, R.P., Buesing, C.M., Helm, J., Gogolewski, S., 1997. Regeneration of diaphyseal bone defects using resorbable poly(L/DL-lactide) and poly(D-lactide) membranes in the Yucatan pig model. J. Orthop. Trauma 11, 551–558.
Oest, M.E., Dupont, K.M., Kong, H., Mooney, D.J., Guldberg, R.E., 2007. Quantitative assessment of scaffold and growth factor-mediated repair of critically sized bone defects. J. Orthop. Res., 941–950.
Park, H., Kang, S.-W., Kim, B.-S., Mooney, D.J., Lee, K.Y., 2009. Shear-reversibly crosslinked alginate hydrogels for tissue engineering. Macromol. Biosci. 9, 895–901.
Pauwels, F., 1960. A new theory on the influence of mechanical stimuli on the differentiation of supporting tissue. The tenth contribution to the functional anatomy and causal morphology of the supporting structure. Zeitschrift für Anat. und Entwicklungsgeschichte 121, 478–515.
Perren, S.M., Cordey, J., 1980. The concept of interfragmentary strain. Curr. Concepts Intern. Fixat. Fract., 63–77.
Porter, B.D., Lin, A.S.P., Peister, A., Hutmacher, D., Guldberg, R.E., 2007. Noninvasive image analysis of 3D construct mineralization in a perfusion bioreactor. Biomaterials 28, 2525–2533.
Robling, A.G., Turner, C.H., 2009. Mechanical signaling for bone modeling and remodeling. Crit. Rev. Eukaryot. Gene Expr. 19, 319–338.
Röntgen, V., Blakytny, R., Matthys, R., Landauer, M., Wehner, T., Göckelmann, M., Jermendy, P., Amling, M., Schinke, T., Claes, L., Ignatius, A., 2010. Fracture healing in mice under controlled rigid and flexible conditions using an adjustable external fixator. J. Orthop. Res. 28, 1456–1462.
Roshan-Ghias, A., Lambers, F.M., Gholam-Rezaee, M., Müller, R., Pioletti, D.P., 2011. In vivo loading increases mechanical properties of scaffold by affecting bone formation and bone resorption rates. Bone 49, 1357–1364.
Roshan-Ghias, A., Terrier, A., Bourban, P.-E., Pioletti, D.P., 2010. In vivo cyclic loading as a potent stimulatory signal for bone formation inside tissue engineering scaffold. Eur. Cell. Mater. 19, 41–49.
Roux, W., 1895. Gesammelte Abhandlungen über Entwickelungsmechanik der Organismen: Bd. Entwicklungsmechanik des Embryo. Wilhelm Engelmann.
Solheim, E., Sudmann, B., Bang, G., Sudmann, E., 2000. Biocompatibility and effect on osteogenesis of poly(ortho ester) compared to poly(DL-lactic acid). J. Biomed. Mater. Res. 49, 257–263.
Tang, D., Tare, R.S., Yang, L.-Y., Williams, D.F., Ou, K.-L., Oreffo, R. O.C., 2016. Biofabrication of bone tissue: approaches, challenges and translation for bone regeneration. Biomaterials 83, 363–382, http://dx.doi.org/10.1016/j.biomaterials.2016.01.024.
Turner, C.H., Warden, S.J., Bellido, T., Plotkin, L.I., Kumar, N., Jasiuk, I., Danzig, J., Robling, A.G., 2009. Mechanobiology of the skeleton. Sci. Signal. 2 (pt3).
Uhrig, B.A., Clements, I.P., Boerckel, J.D., Huebsch, N., Bellamkonda, R.V., Guldberg, R.E., 2014. Characterization of a composite injury model of severe lower limb bone and nerve trauma. J. Tissue Eng. Regen. Med. 8, 432–441.
Wildemann, B., Kandziora, F., Krummrey, G., Palasdies, N., Haas, N.P., Raschke, M., Schmidmaier, G., 2004. Local and controlled release of growth factors (combination of IGF-I and TGF-beta I, and BMP-2 alone) from a polylactide coating of titanium implants does not lead to ectopic bone formation in sheep muscle. J. Control. Release 95, 249–256.
Willett, N.J., Li, M.-T.A., Uhrig, B.A., Boerckel, J.D., Huebsch, N., Lundgren, T.L., Warren, G.L., Guldberg, R.E., 2013. Attenuated human bone morphogenetic protein-2-mediated bone regeneration in a rat model of composite bone and muscle injury. Tissue Eng. Part C. Methods 19, 316–325.
Wolf, S., Janousek, a, Pfeil, J., Veith, W., Haas, F., Duda, G., Claes, L., 1998. The effects of external mechanical stimulation on the healing of diaphyseal osteotomies fixed by flexible external fixation. Clin. Biomech. (Bristol, Avon) 13, 359–364.
Wolff, J., 1892. Das gesetz der transformation der knochen. DMW-Deutsche Medizinische Wochenschriftt.